ELSEVIER

International Journal of Adhesion & Adhesives 21 (2001) 87–99

International Journal of Adhesion & Adhesives

Mode I fracture of epoxy bonded composite joints: 1. Quasi-static loading

I.A. Ashcroft[a,*], D.J. Hughes[b], S.J. Shaw[b]

[a]*Department of Mechanical Engineering, Loughborough University, Loughborough, Leicestershire LE11 3TU, UK*
[b]*Structural Materials Centre, Defence Evaluation and Research Agency, Farnborough, Hampshire GU14 0LX, UK*

Accepted 30 August 2000

Abstract

Mode I constant displacement rate tests were conducted on epoxy-bonded CFRP joints at −50, 22 and 90°C. A comparison of experimental compliance and different beam theory approaches indicated that care needs to be taken when applying beam theory approaches across a wide temperature range. Temperature was seen to influence the mode of fracture which progressed from stable, brittle fracture at low temperatures to slip-stick fracture at room temperature and finally to stable ductile behaviour at elevated temperatures. This behaviour has been attributed to the dependence of critical strain energy release rate on crack velocity for epoxy adhesives and a model for the fracture behaviour of viscoelastic materials has been used to explain these results. The critical strain energy release rate was seen to increase with temperature and the failure locus transferred from predominantly in the composite substrate to predominantly in the adhesive.

Keywords: Carbon-fibre-reinforced-plastic; Epoxy adhesive; Strain energy release rate; Temperature; DCB; SEM

1. Introduction

The use of composite materials in aerospace applications is becoming more widespread due to the improved performance that can be achieved by a reduction in weight. Adhesive bonding is seen as a desirable joining technique for these materials as it can offer substantial benefits over other joining methods such as mechanical fastening. Adhesive bonding offers improved fatigue performance, potential reductions in life-cycle maintenance costs, and also allows for greater flexibility in design. However, greater understanding of the fatigue performance of such bonded structures and, in particular, any degradation of that performance due to adverse environments, is needed for the benefits of adhesive bonding to be fully achieved.

Previous work at DERA in this area has centred on the mixed-mode loaded joints, such as the double-lap and lap-strap joints, that are representative of loading in real aerospace structures [1–3]. In this work it has been shown that both fracture mechanics and strain based failure criteria can be used to predict the fatigue thresholds in long overlap joints in a variety of environments. The total strain energy release rate was found to be a useful failure criterion when applied to joints with a similar mode mix. We are now expanding the range of geometries tested and assessing the approach used by Mall et al. [4–6] and Kinloch and co-workers [7–10] in using mode I fracture data to predict failure in uncracked mixed-mode joints.

The double cantilever beam (DCB) sample has been chosen to generate the mode I fracture data. This is a popular test because of the ease of sample manufacture and testing, coupled with simple analysis methods. Ripling et al. [11–13] first adapted the DCB test for testing structural adhesives and suggested a theory based on a built in beam which neglected the contribution of the adhesive. They suggested that rotation at the assumed built in end could be corrected for by using an empirically derived rotation factor that was added to the measured crack length. Later workers [14–18] modelled the DCB as a beam on an elastic foundation in order to theoretically account for the contribution of the adhesive to the compliance.

The DCB has been used to generate fracture data for composites [19–22], bonded composites [4–8, 23–25]

* Corresponding author. Tel.: +44-1509-223229; fax: +44-1509-223934.
E-mail address: i.a.ashcroft@lboro.ac.uk (I.A. Ashcroft).

0143-7496/01/$ - see front matter
PII: S0143-7496(00)00038-5

and bonded metal joints [9–14, 26–28]. The DCB is frequently used to generate fatigue data as well as quasi-static data. This aspect of our work is covered in more detail in Part 2 of this paper.

In this investigation DCBs composed of carbon fibre-reinforced polymer (CFRP) adherends bonded with an epoxy adhesive were tested in the temperature range -50 to 90°C. This temperature range was selected as typical of the limits to be expected in a supersonic aircraft. The effect of temperature on the fracture energy, the mode of fracture and the locus of failure was evaluated using automated crack measuring techniques and microscopy techniques. A number of analysis methods have been assessed with respect to their applicability across this temperature range and the results have been explained with reference to a model for fracture in a viscoelastic material. Part I of the paper is concerned with quasi-static loading of the DCBs and in Part 2 crack propagation for samples subjected to cyclic loading is described.

2. Theory

The energy criterion for crack growth is based on the work of Griffith [29]. The driving force for crack growth is that the stored elastic strain energy released when the crack grows must be at least as great as the energy required to create the new surfaces. The following equation can be derived for the strain energy release rate, G, in a plate with a through thickness crack, assuming linear elastic behaviour:

$$G = \frac{P^2}{2b}\frac{\mathrm{d}C}{\mathrm{d}a}, \tag{1}$$

where P is the applied load, b the specimen width, a the crack length and C the sample compliance, which is defined by

$$C = \frac{\delta}{P} \tag{2}$$

with δ being the displacement. At failure Eq. (1) becomes

$$G_{\mathrm{Ic}} = \frac{P_{\mathrm{c}}^2}{2b}\frac{\mathrm{d}C}{\mathrm{d}a}, \tag{3}$$

where P_{c} is the load at failure, and G_{Ic} is the critical mode I strain energy release rate or fracture energy. From Eq. (1) it can be seen that the strain energy release rate for any cracked plate can be calculated quite easily once the change in compliance with crack length is known. Two approaches are commonly used to calculate the change in compliance with crack length for a DCB. The first method is to use experimental values of load and displacement in Eq. (2) to obtain a set of values for compliance as a function of crack length throughout the test. The second method uses beam theory to obtain an expression for the compliance in terms of geometry and material properties. A comparison of experimental compliance (from three samples) and compliance calculated by beam theory for the DCB used in the current work at room temperature is shown in Fig. 1. The beam theory compliance was calculated using the approach of Mostovoy et al. [12], given in

$$C = \frac{8a}{bEh^3}(a^2 + h^2), \tag{4}$$

where E is the longitudinal tensile modulus of the adherend, b is the specimen width (25 mm) and h is half the specimen thickness (2 mm). Two values were used for the adherend modulus, the manufacturer's value of 174 GPa and an experimentally determined value of 123 GPa (the derivation of which is described in the discussion section of this paper). The experimental compliance shows considerable scatter and not surprisingly the beam theory compliance using the experimentally derived modulus value provides a good fit to the experimental data. The beam theory compliance using the manufacturer's modulus value does not provide such a good fit to the data and appears to provide a lower bound for the experimental values.

Three different analysis methods were investigated in this work. These consisted of an experimental compliance method (Berry method) [30], and two beam theory methods [31]. The Berry method uses a plot of compliance, C, against crack length, a, on a log–log chart. A straight line fit to this curve gives

$$C = Ka^n, \tag{5}$$

where n is the slope of the curve and K is the intercept. This can be substituted into Eq. (3) to obtain G_{Ic}:

$$G_{\mathrm{Ic}} = \frac{nP_{\mathrm{c}}\delta}{2ba} \quad \text{Berry method.} \tag{6}$$

The first beam theory approach (CBT1) is a load method, where compliance is given by

$$C = \frac{2a^3}{3EI}. \tag{7}$$

The second moment of area of the beam is

$$I = \frac{bh^3}{12}. \tag{8}$$

Differentiating Eq. (7) with respect to a, and substitution into Eq. (3) gives the expression

$$G_{\mathrm{Ic}} = \frac{12P^2a^2}{b^2h^3E} \quad \text{CBT1.} \tag{9}$$

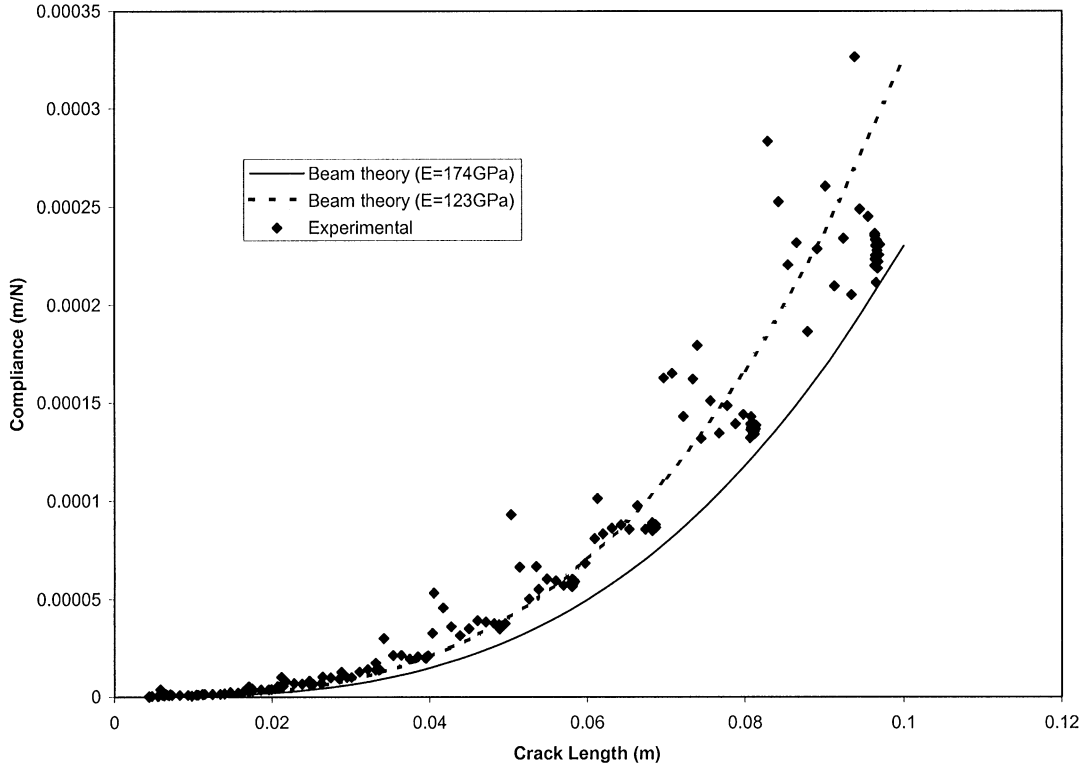

Fig. 1. Comparison of calculated and experimental compliance against crack length.

The second beam theory approach (CBT2) is a displacement method, where the load, P, is given by

$$P = \frac{3\delta EI}{2a^3}. \tag{10}$$

This can be substituted into Eq. (7) to obtain the following equation for G_{Ic}:

$$G_{Ic} = \frac{3P\delta}{2ba} \quad \text{CBT2}. \tag{11}$$

In practice, these beam theory approaches will tend to underestimate the compliance, since the simplified theory assumes that the beams are perfectly built-in. One correction method commonly used to account for the deflection due to the beam-end rotation is to use an assumed increase in crack length a_0 [12,31]. This correction factor can be interpolated from a plot of $C^{1/3}$ vs. a, where a residual crack length will exist at $C^{1/3} = 0$. The residual crack length is then simply added to the measured crack length. All values of strain energy release rate calculated in this work use an end-correction term calculated in this manner.

An Excel macro was written using Visual Basic for Applications to aid analysis using all the different approaches. This requires the input of test variables such as specimen dimensions and pre-crack length, before the strain energy release rates are calculated from the data file using all the different methods. The results are placed into an Excel spreadsheet and the graphs automatically plotted to enable simple and direct comparisons to be made.

3. Experimental

3.1. Sample preparation

Samples were produced by adhesive bonding cured panels of CFRP. The composite was prepared from unidirectional pre-preg consisting of intermediate modulus graphite fibres in a BMI/epoxy matrix. A unidirectional lay-up of 16 plies at 0° was used to produce 2 mm thick panels. These were autoclave cured at 180°C for 60 min. The mechanical properties of the composite used in the analyses were those supplied by the manufacturer and are shown in Table 1. The adhesive used was a toughened epoxy film which was approximately 0.2 mm thick and was supported by a non-woven nylon carrier. The adhesive was autoclave cured at 120°C for 60 min. The mechanical properties of the adhesive were obtained by testing bulk adhesive samples, which were manufactured by curing multiple layers of the carried film adhesive [32]. Typical tensile stress–strain curves at different temperatures are shown in Fig. 2.

The cured CFRP panels were scanned ultrasonically prior to bonding to check for defects. The panels were then grit-blasted with alumina grit and degreased with

acetone before being laid up with the adhesive film. A thin film of PTFE (nominally 10 μm) was placed at the bondline at the loading end of the joint to act as a starter crack. Brass hinges were bonded to the samples to enable load application to the joint. Strips of PTFE film were placed over the hinge during bonding to retain freedom of movement.

To enable accurate measurement of crack length throughout the test 'Krak Gages' were bonded to the sides of the samples over the bondline. These are thin strips of constantan, which are designed to tear as the sample cracks. The dimensions of the double cantilever beam specimen used in this work can be seen in Fig. 3.

3.2. Testing

Testing was carried out using servohydraulic machines fitted with computer control and data logging. Crack length was measured using the commercial *Fractomat-Krak Gage* system from Rumul. The 'Fractomat' is used to excite the gauge and to monitor the crack length. When a crack grows in the sample the gauge tears, increasing the path length for the current across the gauge. This causes an increase in resistance that is measured by the Fractomat and converted to a crack length [33,34]. A calibrated travelling microscope was used to check the calibration of the Krak Gages to an accuracy of 0.01 mm. The analogue nature of readings from the 'Krak Gage' give it an indefinite resolution and the manufacturers claim an accuracy of greater than 2%. The control computer was used to monitor crack length via a strain channel on the test machine. Constant displacement rate testing was conducted using a ramp rate of 1 mm per minute. Tests were conducted at $-50 \pm 2^{\circ}C$, room temperature ($22 \pm 2^{\circ}C$), and $90 \pm 2^{\circ}C$ and a minimum of 3 tests were performed at each temperature. After testing, optical microscopy was used to study the locus of failure and to examine the appearance of the fracture surface. Samples for SEM analysis were then extracted using a diamond saw, and mounted on metal stubs. These were gold coated to ensure electrical conductivity.

Table 1
Mechanical properties of CFRP

Property	Unidirectional laminate	Units
E_1	174	GPa
E_2	9.64	GPa
G_{12}	7	GPa
v_{12}	0.36	
v_{21}	0.02	

4. Results

4.1. Room-temperature testing

Fig. 4 shows the results of a typical constant displacement rate test conducted at room temperature. As expected, the load is seen to decrease with increasing crack length during the test. However, it is apparent from this plot that growth is not continuous, but instead proceeds as a succession of rapid growth and arrest phases. This is commonly referred to as stick-slip growth. It can also be

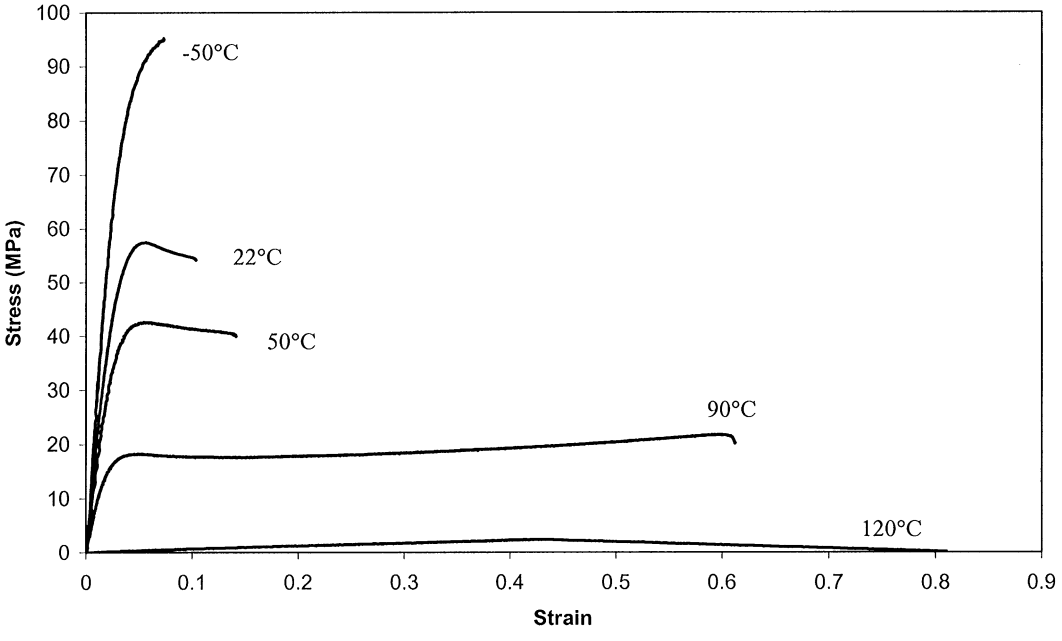

Fig. 2. Mechanical properties of the adhesive as a function of temperature.

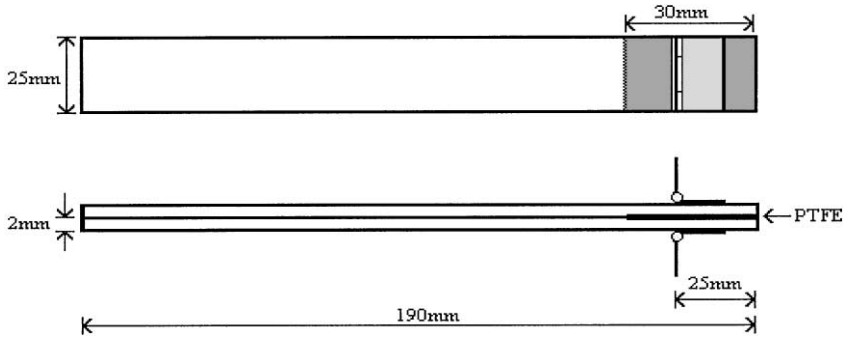

Fig. 3. Dimensions of double cantilever beam specimen.

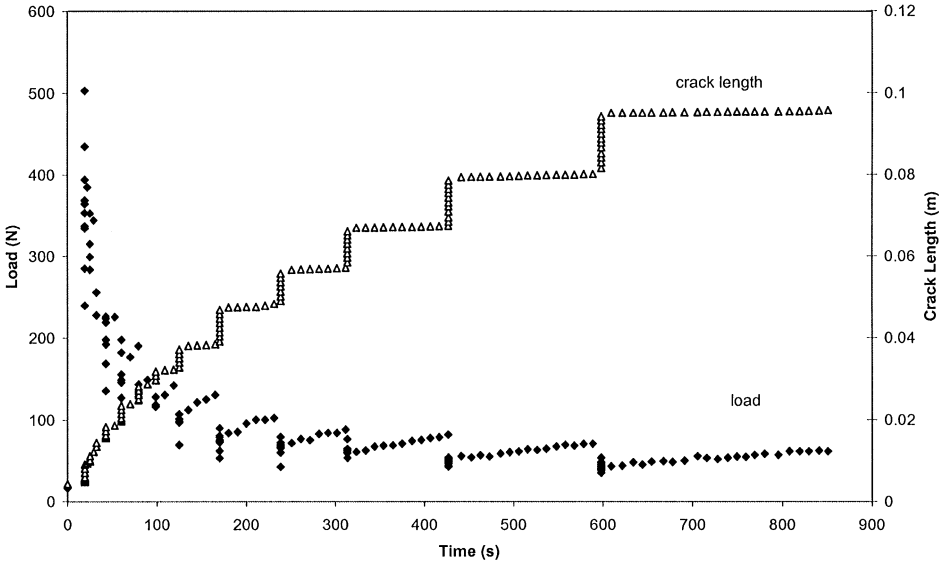

Fig. 4. Typical plot of load and crack length vs. time for a DCB tested at room temperature.

seen that there is an increase in the size of the steps as the crack progresses. We can calculate two critical strain energy release rates from this data. One associated with crack initiation, G_i and one associated with crack arrest, G_a. The results of the three different analyses for the calculation of the strain energy release rate associated with crack initiation can be seen in Fig. 5. In all cases G is high in the early stages of the test, then levels out after 5–20 mm of crack growth. The critical strain energy release rate then remains approximately constant to the end of the test. There is reasonably good correlation with all three methods. Fig. 6 shows a comparison between the strain energy release rates for initiation and arrest calculated using the Berry method. It can be seen that G_i is in the range 300–500 J/m^2 and G_a is in the range 150–250 J/m^2.

A typical failure surface produced by a constant displacement rate test at 22°C can be seen in Fig. 7. The starter crack formed by the PTFE insert can be seen at the right hand end of the specimen, with crack growth running from right to left. An obvious stick-slip pattern can be seen on the fracture surface of this specimen. Phases of fast crack growth are visible as dark areas where failure in the composite is the dominant failure mechanism. Microscopic study showed that the composite failed in the ply adjacent to the adhesive. The fracture surface on the composite side consisted of matrix with exposed fibres whereas the fracture surface on the adhesive side consisted of matrix with imprints of the fibres from the opposite fracture surface. This indicates that the crack does not break through the fibres. Therefore, matrix failure and removal of fibres from the matrix dominate fracture in the composite. Some apparent interfacial failure was also observed in the fast fracture region. Electron microscopy indicated that this was in fact failure on an undulating path in an interfacial region [3]. The regions of fast fracture are separated by white bands, which are small areas where cohesive failure of the adhesive is dominant. These areas are the sites of slow crack growth in the load build-up phase. Higher magnification

showed that these were mixed failure sites with some composite failure and apparent interfacial failure also evident.

4.2. High-temperature testing

Fig. 8 shows the change in load and crack growth with time during a test at 90°C. Crack growth is more continuous than at 22°C, though some small discontinuities can still be seen. The load also decreases more steadily throughout the test. A comparison of the different analysis approaches is shown in Fig. 9 for a fatigue test at 90°C. The difference between the results produced by the different analysis methods is much greater at 90°C than at 22°C.

The failure surface of a specimen tested at 90°C is shown in Fig. 10. The surface shows cohesive failure of the adhesive to be the dominant failure mode. The striations, indicative of slip-stick behaviour, cannot be seen on this sample. The starter crack is visible at the right-hand end of the specimen, whilst the darker region at the left-hand end was the result of pulling the fracture surfaces apart at room temperature after testing. Also visible in the fracture surface are dark strips running in the direction of crack propagation, suggesting small regions of composite or apparent interfacial failure.

Fig. 11 shows the micrograph of a fracture surface from a constant displacement rate test at 90°C. The fracture surface shown depicts all the main failure modes encountered in this work. In the centre of the photograph clean carbon fibres are visible where matrix resin has been removed from the composite surface. Also the fibre at the right-hand side of the image has fractured. Surrounding the area of matrix removal is a region of apparent interfacial failure, showing remnants of adhesive. At the edges of the micrograph can be seen cohesive failure of the adhesive, complete with evidence of the rubber toughening particles in the form of cavities.

4.3. Low-temperature testing

The results of a typical constant displacement rate test at −50°C can be seen in Fig. 12. Crack growth is

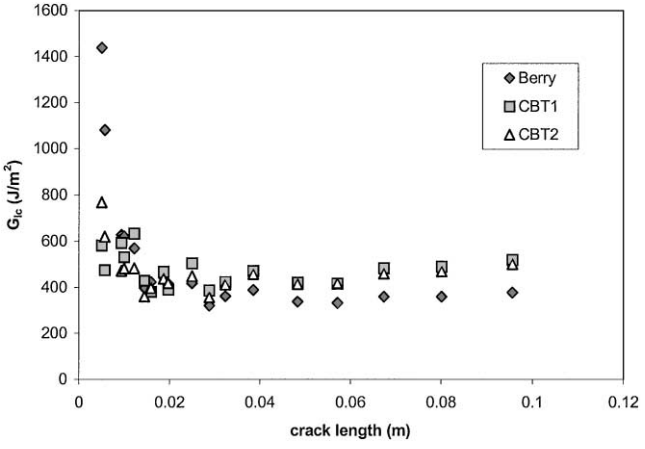

Fig. 5. Comparison of methods used to calculated G at room temperature.

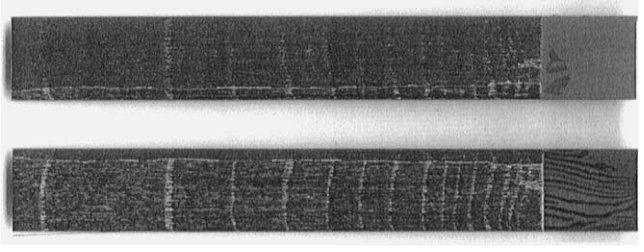

Fig. 7. Fracture surface of a DCB tested at room temperature.

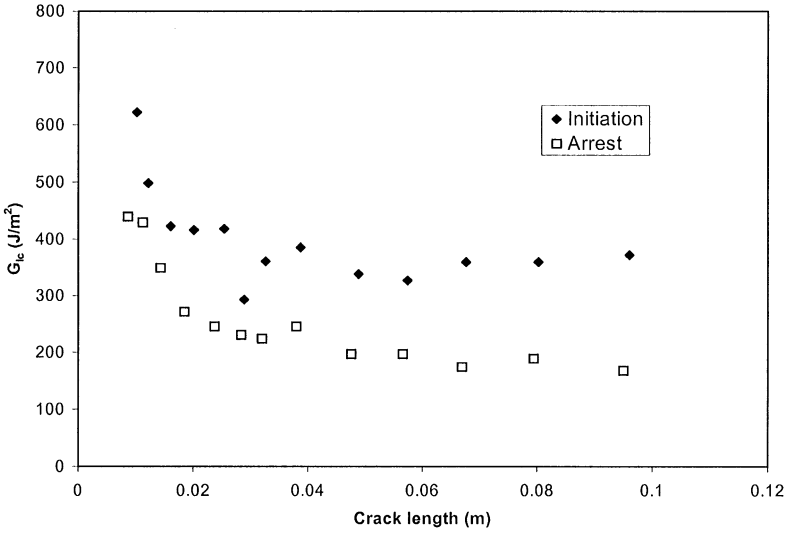

Fig. 6. Comparison of critical strain energy release rates for crack initiation and crack arrest.

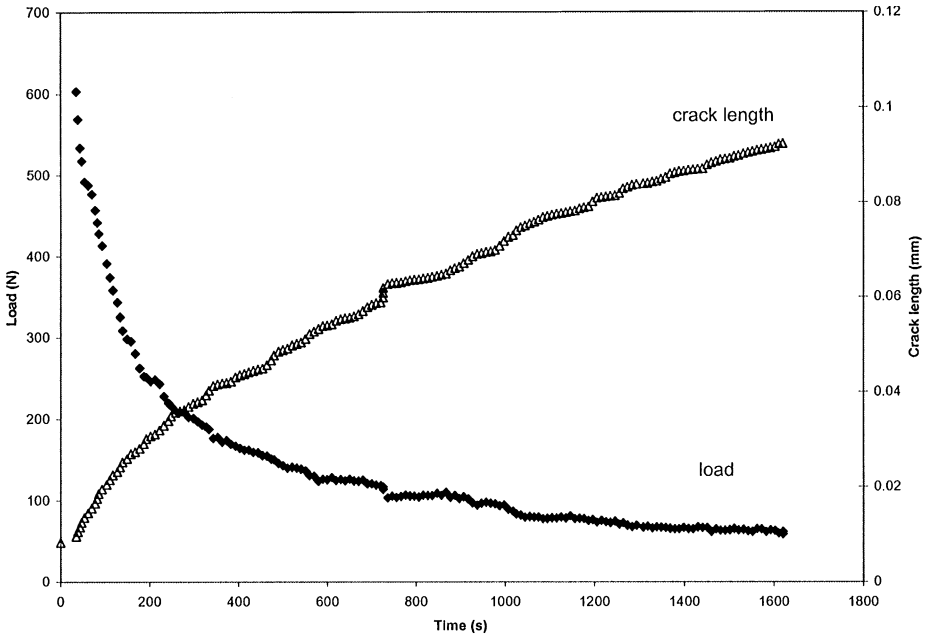

Fig. 8. Typical plot of load and crack length vs. time for a DCB tested at 90°C.

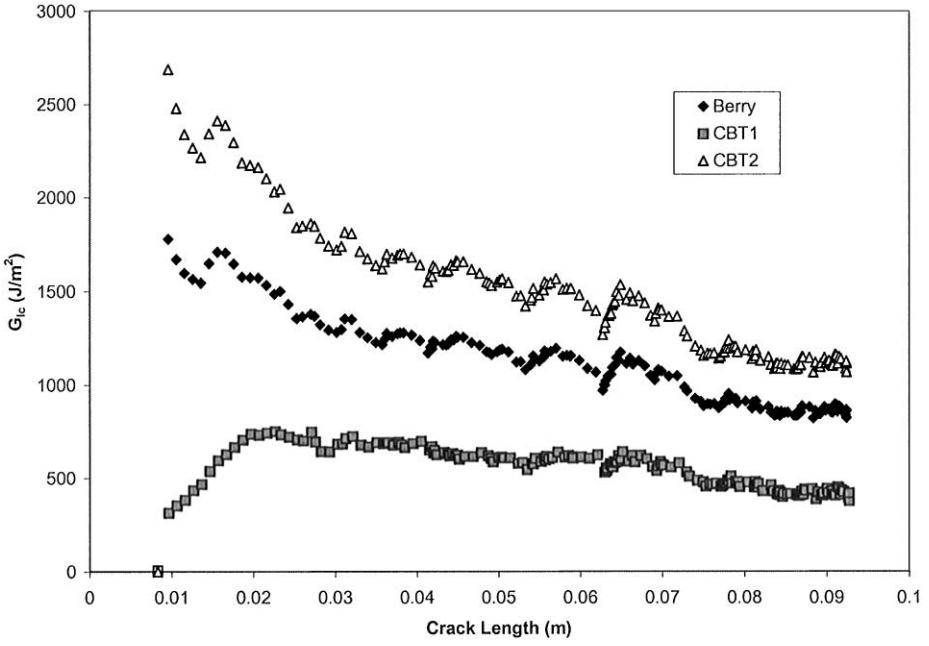

Fig. 9. Comparison of methods used to calculate G at 90°C.

increasing steadily whilst load decreases throughout the test. Small discontinuities can be seen in the crack growth, particularly at higher crack lengths, which is indicative of some variation in crack velocity. However, this is far less marked than at room temperature.

The results of the different analysis methods are shown in Fig. 13. The Berry method and the beam theory displacement method (CBT2) show good correlation, with a decrease in G_{Ic} at the beginning of the test and a slight increase near the end. The value for G_{Ic} is in the range 200–300 J/m^2. The beam theory load method (CBT1) greatly exaggerates the trends shown in the other two curves and gives a value for G_{Ic} more than double that of the other methods, in the range 600–1000 J/m^2.

The failure surface of a joint tested at -50°C is shown in Fig. 14. Crack growth runs from the starter crack at

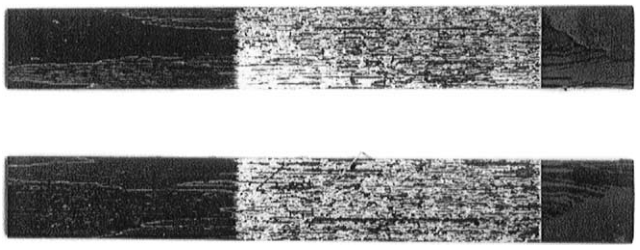

Fig. 10. Failure surface of a DCB tested at 90°C.

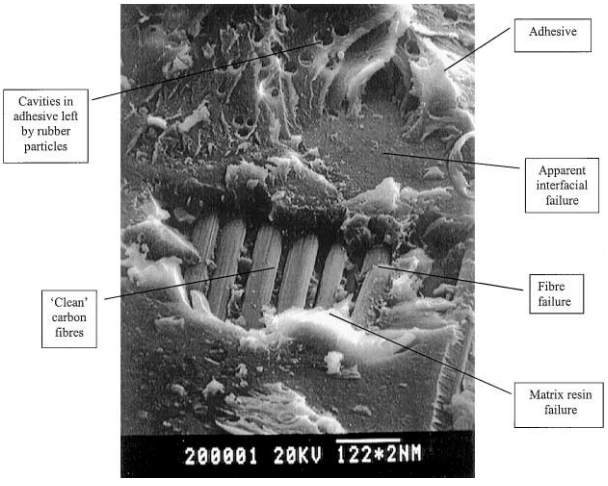

Fig. 11. Scanning electron micrograph of a failure surface in a DCB tested at 90°C.

the right-hand end of the specimen and the dominant failure mode is fracture of the composite. The lighter coloured regions indicate some apparent interfacial failure.

5. Discussion

5.1. Comparison of analysis methods

All three analysis methods gave similar results at 22°C, but at 90°C there was some difference between the values. The experimental compliance (Berry) method and the beam theory displacement method (CBT2) showed a reasonable correlation with one another, but the beam theory load method (CBT1) gave considerably lower values of G_{Ic}. This may be due to the simplification of assuming the longitudinal stiffness of the composite does not change in the test temperature range. If the stiffness of the composite beam decreased at elevated temperatures the stiffness value used in Eq. (9) would be larger than the actual stiffness and so the calculated value of G_{Ic} would be too small. At -50°C the Berry and CBT2 methods showed very good correlation, but the CBT1 method predicted much larger values for G_{Ic}. Again this is most likely due to the stiffness values used in Eq. (9). At low temperatures the stiffness of the adherend might be expected to increase and the room temperature modulus value used in Eq. (9) would be too small. The calculated value for G_{Ic} would therefore be too great. An 'effective' modulus value can be calculated from Eq. (7) by fitting

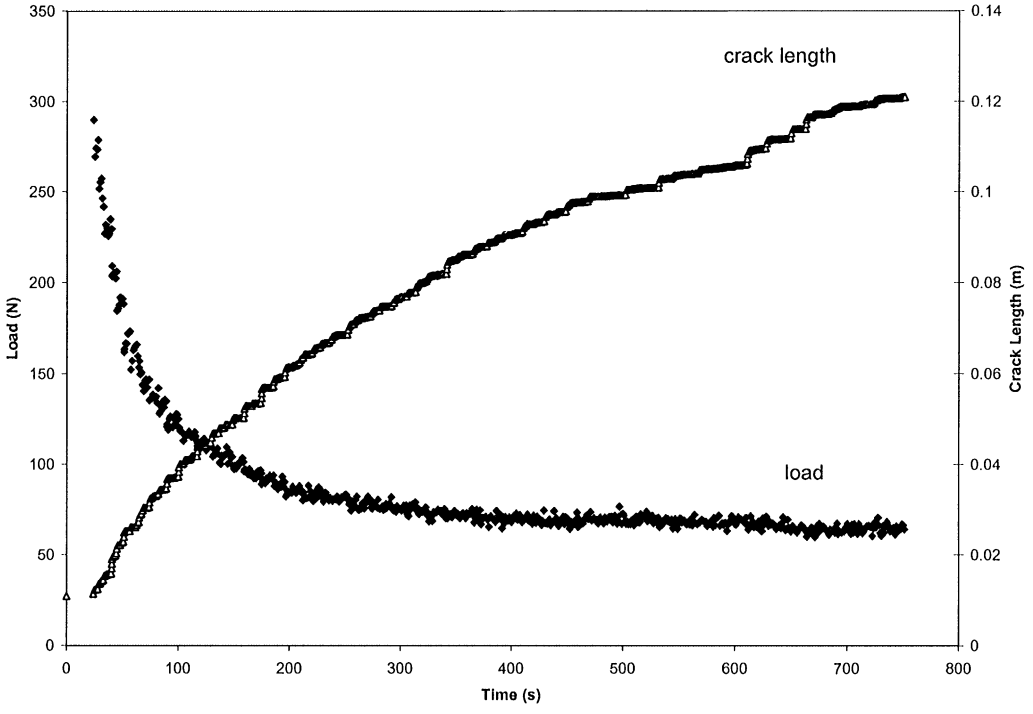

Fig. 12. Typical plot of load and crack length vs. time for a DCB tested at -50°C.

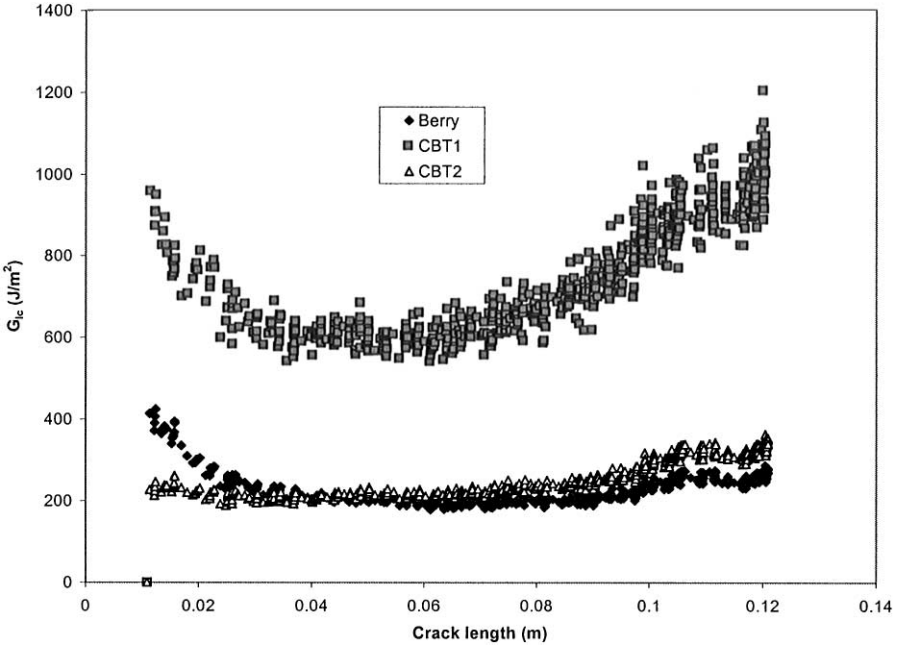

Fig. 13. Comparison of methods used to calculate G at -50°C.

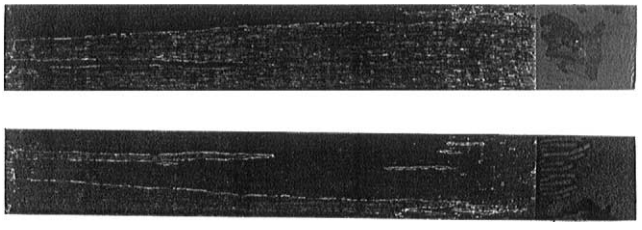

Fig. 14. Failure surface of a DCB tested at -50°C.

a straight line to a plot of experimental compliance against the cube of the measured crack length. This method gives mean moduli of 118, 123 and 341 GPa at 90, 22 and -50°C, respectively. Compared to the manufacturer's modulus value these experimentally determined values appear rather low at 90 and 22°C and high at -50°C. This raises further doubts about the applicability of the simple beam theory approach across this temperature range for this type of sample and an experimental compliance approach is therefore recommended.

Each analysis shows that G_{Ic} is higher at the start of the test. This is because the starter crack formed by the PTFE film is relatively blunt and therefore more difficult to propagate. On loading, a plastic zone will form ahead of the 'blunt' crack, which will also influence initial crack propagation. As the crack sharpens, the value of G_{Ic} decreases to an approximately constant level. However this was not the case for the results at 90°C, where G_{Ic} tended to continue to decrease along the bond line. Two factors may contribute to this observation. Firstly, the reduced stiffness/increased compliance of the joints and increased toughness of the adhesive at this temperature will require increased displacements to propagate failure. Secondly there is a marked increase in plasticity of the adhesive at 90°C, as clearly indicated in Fig. 2, and so tests at this temperature may have exceeded the limits of linear elastic fracture mechanics. It is intended that finite element modelling and evaluation using the J-integral approach will be used to assess the effects of non-linearity at high temperatures in future work.

5.2. Stick-slip behaviour

Under constant displacement rate testing it was seen that at 22°C there was stick-slip behaviour. This behaviour is characterised by a slow growth region as load increases, which occupies most of the time of the propagation. At a critical strain energy release rate (G_i) rapid, unstable crack growth occurs. This occupies most of the crack propagation in terms of distance. During unstable crack growth the crack velocity greatly exceeds the machine imposed crack growth rate and hence load (and strain energy release rate) decreases. When a critical strain energy release rate for this fast crack growth (G_a) is reached fast crack growth stops. We then return to a period of slow crack growth.

Stick-slip behaviour can be explained by reference to the relationship between strain energy release rate and crack velocity in viscoelastic materials. The kinetics of crack growth in viscoelastic materials has been described by Maugis [35,36] using

$$G - 2\gamma = 2\gamma\Phi(a_T v), \tag{12}$$

where γ is the intrinsic fracture energy, Φ is a non-dimensional loss function, v is the crack velocity and a_T is the Williams–Landel–Ferry shift factor [37]. The use of the WLF shift factor allows results at various temperatures to be shifted to a reference temperature, T_S in order to construct a master curve. A given value of $a_T v$ can correspond to a low v at high temperature or a high v at low temperature. Eq. (13) can be used to estimate the shift factor [38]

$$\log a_T = \frac{C_1(T - T_S)}{C_2 + T - T_S}, \tag{13}$$

where C_1 and C_2 are constants. From Eq. (12) it can be seen that when $G > 2\gamma$ the crack has a velocity which depends on the crack driving force, $G - 2\gamma$. At a critical velocity, v_c, $d\Phi/dv$ becomes negative and a velocity jump is observed. At this point G_c is defined which is really a criterion for crack speed discontinuity.

Maugis [36] proposed that in a viscoelastic material, the superposition of the effects of viscoelastic losses and the dynamic effects of brittle fracture gave two positive branches in the plot of G against crack velocity separated by a negative branch, as shown in Fig. 15. Stick-slip behaviour occurs when we attempt to impose a crack velocity, v_{imp}, on the negative branch of the curve in Fig. 15. In a constant displacement rate test G will increase with displacement for a constant crack length. In Fig. 15 sub-critical crack growth may occur when G exceeds 2γ, although it may not be discernible until G has increased further. As we are attempting to impose a crack velocity of v_{imp}, G will continue to rise until we reach a critical crack velocity, v_c, at A. We cannot follow the curve on the negative branch because if the crack velocity increases the resistance to crack propagation decreases, resulting in an unstable acceleration of the crack. We therefore get a velocity jump onto the next positive branch of the curve at B. Therefore, G_i is actually a criterion for a change in crack velocity. However, the crack velocity is now higher than v_{imp} and slows to C. This is still higher than our imposed velocity so we get another velocity jump to D where the crack appears to be arrested. However, this is in fact in the slow crack growth regime. Of course, the crack velocity is now less than v_{imp} so the cycle is repeated. It can be seen from the above that stick-slip behaviour is controlled by the imposed velocity. An imposed velocity above v_2 or below v_c will give stable growth.

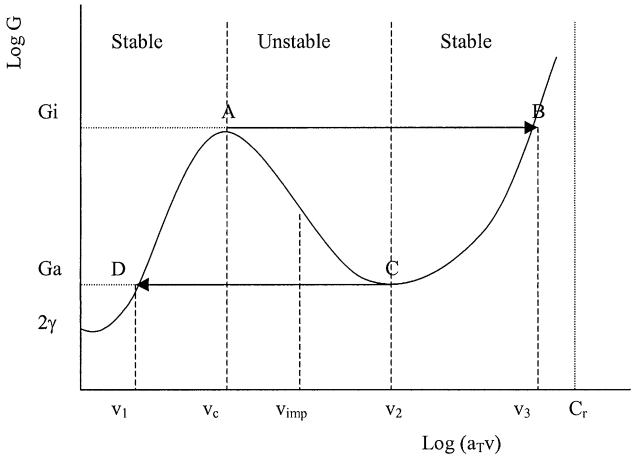

Fig. 15. Schematic figure showing the variation in strain energy release rate with crack velocity for a viscoelastic material.

An attempt to construct an experimental plot of G against v has been made using a secant method to calculate crack velocity from the plots of crack length against time. Crack velocity as a function of crack length is thus obtained and can be plotted against the value of G calculated from the measured sample compliance. A number of such plots are shown in Fig. 16. As expected, some scatter can be seen, however, repeatability is surprisingly good and the general shape of the plot is as predicted. A slow growth region can be seen until G reaches a value of approximately $300\,J/m^2$ at a crack velocity of about 0.5 mm/min. The crack velocity then increases rapidly until G has fallen to a value between 150 and $200\,J/m^2$, at which point crack velocity again falls below 0.5 mm/min. However, it is recognised that further experimental data is required to fully validate this model.

In the case of epoxy adhesives, stick-slip behaviour has been attributed to plastic crack blunting at the crack tip, which is controlled by the yield behaviour [39–41]. Yamini and Young [42] suggested that after crack arrest, a plastic zone forms at the crack tip. Slow growth is seen as the crack progresses through this plastic zone which is followed by fast growth through 'virgin' material. They supported this view by correlating the regions of slow growth in their samples with the calculated plastic zone size. This model can be used to explain the change in fracture path from the adhesive in the 'stick' region to the composite in the 'slip' region. At room temperature, the adhesive has a lower yield strength than the composite, so the sub-critical crack growth, which is dominated by viscoelastic deformation, would be expected to be in the adhesive. However, at high crack velocities where fracture is essentially elastic, failure is in the more brittle composite matrix. This view is confirmed by the fact that G_a at 22°C is approximately the same as G_c at -50°C.

Once we have obtained values for G_i and G_a we can easily predict the stick-slip behaviour in any joint if we make the simplifying assumptions that there is no crack growth below G_i and that the fast crack growth is instantaneous compared with machine displacement. For example, in order to predict the stick-slip behaviour in the DCBs, Eq. (10) was substituted into Eq. (9) to give

$$G = \frac{3\delta^2 E h^3}{16a^4}. \tag{14}$$

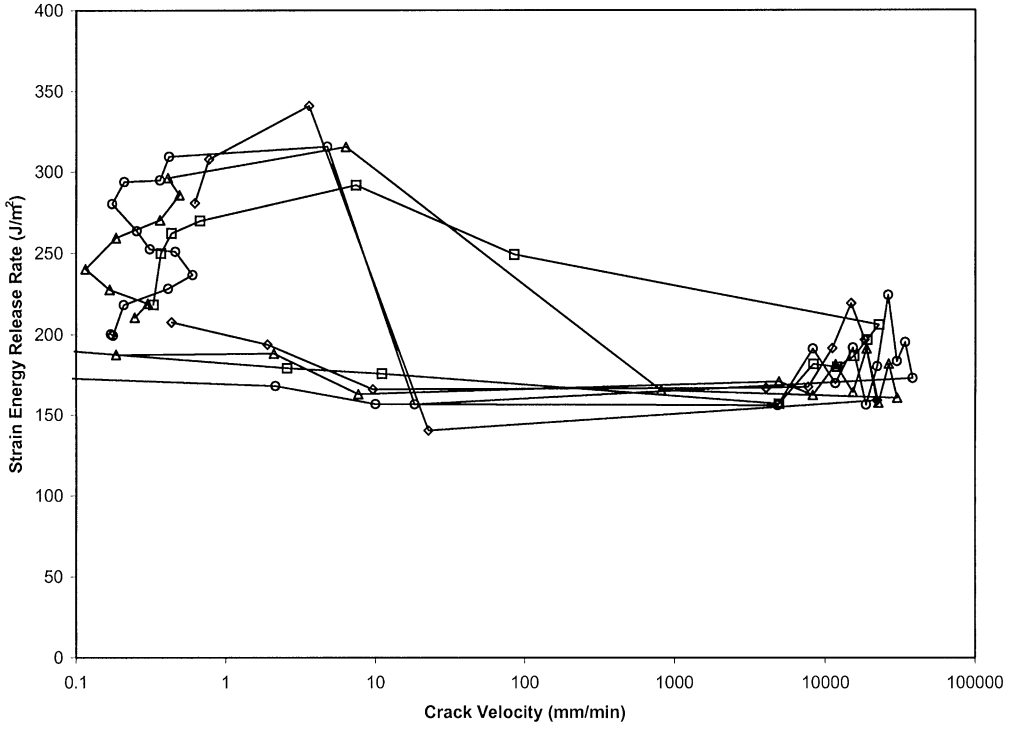

Fig. 16. Experimental plots of strain energy release rate against crack velocity for a DCB tested at room temperature.

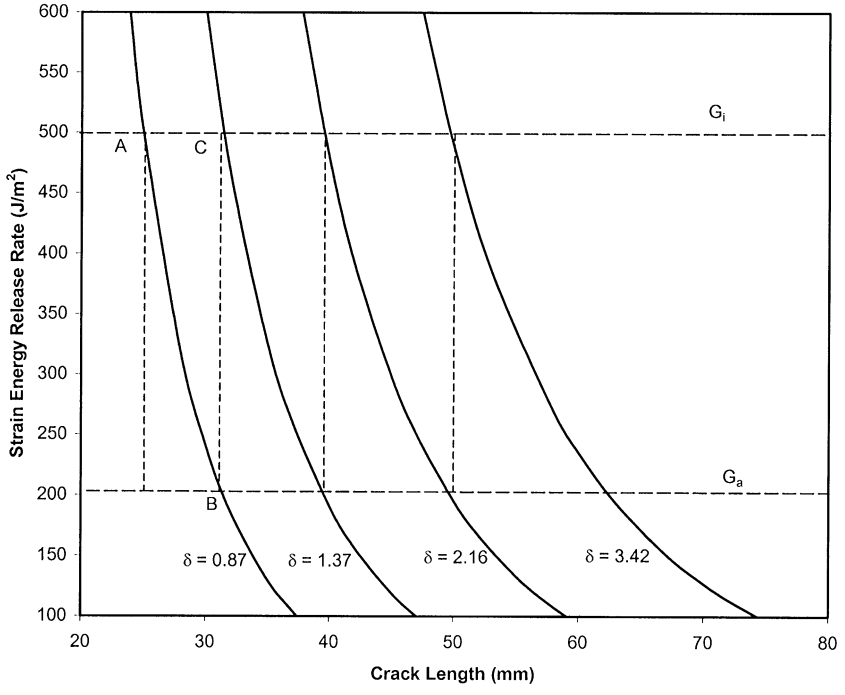

Fig. 17. Figure showing how stick-slip behaviour can be predicted for a bonded joint.

From Fig. 17 we can see that if we start with an initial crack length of 25 mm and start to monotonically increase displacement, there is no change in crack length until we reach G_i (500 J/m^2 in this example) at A. The displacement at which fast crack growth occurs can be calculated by substituting G_i into Eq. (14) for a crack length of 25 mm. We then get rapid crack growth at constant machine displacement until G has decreased to G_a (200 J/m^2 in this example). The curve A–B can be generated from Eq. (14) by substituting the displacement

calculated previously if we assume that further displacement is negligible in the time taken for the fast growth phase. The end point of the crack jump can be calculated by substituting G_a into Eq. (14). This process is repeated along the length of the sample and it can be seen that it is predicted that the size of the crack jumps increase as the crack grows, which is in agreement with the experimental results shown in Fig. 4. The loads at which the crack jumps occur can also be calculated using Eq. (10). This method could be applied to any joint in which we can calculate the strain energy release rate as a function of crack length and would be useful in predicting the likelihood of a catastrophic failure in the structure.

5.3. Effect of temperature

The model described above can also be used to explain the observed variation in crack behaviour with temperature. As temperature decreases, the yield stress of the adhesive increases and viscoelastic effects decrease. We can simulate the effect of decreasing temperature in Fig. 15 by increasing our imposed crack velocity. It can be seen that when v_{imp} is greater than v_2 we will have a crack velocity jump at v_c but then crack growth will be stable as it will be on a positive branch of the G–v curve. The fracture will be elastic and will be relatively independent of temperature and rate until the Rayleigh velocity, C_r, is approached. Alternatively, if temperature increases then we can simulate this by decreasing v_{imp}. When v_{imp} is less than v_c we will have stable crack growth. However, in this case the crack growth is dominated by viscoelastic deformation and the measured G_c will be highly dependent on rate and temperature.

It can be seen from Table 2 that temperature has a marked effect on the mode I fracture toughness. The value of G_{Ic} is lowest at -50°C at 200–300 J/m^2. This corresponds quite closely to G_a at room temperature, indicating that the mainly elastic failure in the composite is temperature independent. Values of G_{Ic} in the literature [43] for interlaminar failure of the composite used in this work are 220–280 J/m^2 at room temperature. This agrees well with the results for the bonded composites when failure was predominantly in the composite. At 22°C the value of G_i is 400–600 J/m^2. A value of G_{Ic} of 1550–1700 J/m^2 has been reported in the literature [10] for 100% cohesive failure of the same adhesive when bonded to aluminium adherends and tested at room temperature. G_i for the bonded composite can therefore be seen to be in between the reported values for the composite and adhesive, which is consistent with the failure mode. G_{Ic} was greatest at 90°C where values between 1000 and 2000 J/m^2 were recorded. From Table 2 it can also be seen that the amount of scatter in the results increases with temperature.

It was noted that there was a change in the failure mode as the test temperature increased. At -50°C the dominant failure mode was brittle fracture in the top ply of the composite adherends. Increasing the temperature to 90°C saw the dominant failure mode change to ductile failure of the adhesive. This can be attributed to differences in the mechanical behaviour of the toughened epoxy of the adhesive and the BMI-based composite matrix and to the fact that the composite matrix is a high temperature material with a T_g of approximately 200°C whereas the adhesive has a T_g of only about 130°C.

b

Table 2
Summary of results

Temperature (°C)	Crack growth	G_{Ic} (J/m^2)	Dominant failure mode
-50	Stable: brittle fracture	250 ± 50	C[a]
22	Stick-slip: unstable region	200 ± 50	C
22	Stick-slip: stable region	500 ± 100	C and A[b]
90	Stable: ductile fracture	1500 ± 500	A

[a] C = failure in composite.
[b] A = failure in adhesive.

6. Conclusions

The various methods available for calculating mode I strain energy release rates from double cantilever beam joint geometries can result in different values. This is particularly true for beam theory related procedures when uncertainty may exist as to appropriate material properties, or if there is likelihood of significant joint non-linearity. Under such circumstances an experimental compliance method is the recommended option.

In the joints studied, modes of fracture, locus of failure and fracture energy are all influenced by test temperature. At low temperatures (-50°C) stable, brittle fracture predominates whereas at 20°C a discontinuous stick-slip form of crack growth exists. An elevated temperature of 90°C promotes stable ductile crack growth.

Increasing temperature increases fracture energy together with locus of failure changing from predominantly within the composite at -50°C to cohesive within the adhesive at 90°C.

These observations are adequately explained by reference to a model relating to fracture in viscoelastic materials and a method for predicting stick-slip behaviour is outlined.

References

[1] Ashcroft IA, Gilmore RB, Shaw SJ. Cyclic fatigue and environmental effects with adhesively bonded joints. 83rd Meeting of the AGARD Structures and Materials Panel. Florence, Italy: NATO, 1996.

[2] Ashcroft IA, Hughes DJ, Shaw SJ. Mixed mode fatigue testing of bonded composite joints. Proceedings of the Fifth International Conference on Structural Adhesives in Engineering. Bristol: Institute of Materials, 1998.
[3] Ashcroft IA, Hughes DJ. Fatigue of epoxy adhesives. DERA Technical Report DERA/MSS1/CR990289/1.0, March 1999.
[4] Mall S, Johnson WS, Everett Jr RA. Cyclic debonding of adhesively bonded composite. In: Mittal KL editor, editor. Adhesive joints: their formation, characteristics and testing. New York: Plenum Press, 1984. p. 639–58.
[5] Mall S, Johnson WS. Characterisation of mode I and mixed mode debond failure of adhesive bonds between composite adherends. In: Composite materials: testing and design, vol. ASTM STP 893. Philadelphia: American Society for Testing and Materials, Philadelphia, 1986. p. 332–4.
[6] Mall S, Rezaizdeh MA, Ramamurthy G. Interaction of mixed mode loading on cyclic debonding in adhesively bonded composite joints. ASME Paper No. 85-WA/Mats-1, presented at ASME Winter Annual Meeting, Miami Beach, Florida, November 1985.
[7] Kinloch AJ, Osiyemi SO. Predicting the fatigue life of adhesively bonded joints. J Adhesion 1993;43:79–90.
[8] Charalambides MN, Kinloch AJ, Mathews FL. Strength prediction of bonded joints. 83rd Meeting of the AGARD Structures and Materials Panel. Florence, Italy: NATO, 1996.
[9] Jethwa JK, Taylor AC, Kinloch AJ, Curley AJ. The fatigue and durability behaviour of automotive adhesives. Part III: predicting the service life. J Adhesion 1997;66:39–59.
[10] Little MSG. The durability of structural adhesive joints. Ph.D. thesis, Imperial College, London, 1999.
[11] Ripling EJ, Mostovoy S, Patrick RL. Measuring fracture toughness of adhesive joints. Mater Res Stands 1964;4:129–34.
[12] Mostovoy S, Crosley PB, Ripling EJ. Use of crack-line-loaded specimens for measuring plane strain fracture toughness. J Mater 1967;2:661–81.
[13] Ripling EJ, Corten MT, Mostovoy S. Fracture mechanics: a tool for evaluating structural adhesives. J Adhesion 1971;3:107–23.
[14] Chow CL, Woo CW, Sykes JL. On the determination and application of COD to epoxy-bonded aluminium joints. J Strain Anal 1979;14:37–42.
[15] Ben Ouezdou M, Chudnovsky A. Stress and energy analysis of toughness measurements for adhesive bonds. Eng Fract Mech 1988;29:253–61.
[16] Penado FE. A closed form solution for the energy release rate of the double cantilever beam specimen with an adhesive layer. J Compos Mater 1993;27:383–407.
[17] Olsson R. A simplified improved beam analysis of the DCB specimen. Comput Sci Technol 1992;43:329–38.
[18] Ben Oezdou M, Chudnovsky A, Abdelsamie M. Re-evaluation of adhesive fracture energy. J Adhesion 1988;25:169–83.
[19] Rybicki EF, Hernandez TD, Deibler JE, Knight RC, Vinson S. Mode I and mixed mode energy release rates values for delamination of graphite/epoxy test specimens. J Compos Mater 1987;21:105–23.
[20] Prel YJ, Davies P, Benzeggah ML, de Charentenay F. Mode I and mode II delamination of thermosetting and thermoplastic composites. In: Composite materials: fatigue and fracture, vol. ASTM STP 1012. Philadelphia: American Society for Testing and Materials, 1989. p. 251–69.
[21] Ducept F, Davies P, Gamby D. An experimental study to validate tests used to determine mixed mode failure criteria of glass/epoxy composites. Composites A 1997;28:719–29.
[22] Truss RW, Hine PJ, Duckett RA. Interlaminar and intralaminar fracture toughness of uniaxial continuous carbon fibre/epoxy composites. Composites A 1997;28:627–36.
[23] Ripling EJ, Santner JS, Crosley PB. Fracture toughness of composite adherend adhesive joints under mixed mode I and III loading. J Mater Sci 1983;18:2274–82.
[24] Chai H. On the correlation between the mode I failure of adhesive joints and laminated composites. Eng Fract Mech 1986;24:413–31.
[25] Mangalgiri PD, Johnson WS, Everett Jr RA. Effect of bond thickness on fracture, fatigue strength of adhesively bonded composite joints. J Adhesion 1987;9:263–88.
[26] Gledhill RA, Kinloch AJ. Failure criterion for the fracture of structural adhesive joints. Polymer 1976;17:727–31.
[27] Kinloch AJ, Shaw SJ. The fracture resistance of a toughened epoxy adhesive. J Adhesion 1981;12:59–77.
[28] Dillard DA, Wang JZ, Parvatareddy H. A simple constant strain energy release rate loading method for double cantilever beam specimens. J Adhesion 1993;41:33–50.
[29] Griffith AA. Philos Trans Roy Soc 1920;A221:163.
[30] Davies P. Protocols for interlaminar fracture testing of composites. European Structural Integrity Society: Polymers and Composites Task Group, 1992.
[31] Hashemi S, Kinloch AJ, Williams JG. Corrections needed in double-cantilever beam tests for assessing the interlaminar failure of fibre-composites. J Mater Sci Lett 1989;8:125.
[32] Ashcroft IA, Nelson LJ, Shaw SJ. The effect of environment and loading rate on the mechanical properties of an epoxy film adhesive. Proceedings of the Adhesion '99, IOM Communications, 1999. p. 211–16.
[33] Liaw PK, Logsdon WA, Roth LD, Hartmann HR. In: Cullen WH, Landgraf RW, Kaisand LR, Underwood JH. editors Krakgages for automated fatigue crack growth rate testing: a review, vol. ASTM STP 877. Philadelphia: American Society for Testing and Materials, 1985. p. 177–96.
[34] Pankevicius ER, Spicer M. Technique and apparatus for automatic monitoring of crack propagation along glue lines. J Mater Sci 1990;25:3079–82.
[35] Maugis D, Barquins M. Fracture mechanics, the adherence of viscoelastic bodies. J Phys D: Appl Phys 1978;11:1989–2023.
[36] Maugis D. Subcritical crack growth, surface energy, fracture toughness, stick–slip and embrittlement – a review. J Mater Sci 1985;20:3041–73.
[37] Ferry JD. Viscoelastic properties of polymers. New York: Wiley, 1961.
[38] Williams ML, Landers RF, Ferry JD. J Am Chem Soc 1955;77:3701.
[39] Yamini S, Young RJ. Stability of crack propagation in epoxy resins. Polymer 1977;18:1075–80.
[40] Gledhill RA, Kinloch AJ, Yamini S, Young RJ. Relationships between mechanical properties of and crack propagation in epoxy resin adhesives. Polymer 1978;19:574–82.
[41] Kinloch AJ, Williams JG. Crack blunting mechanisms in polymers. J Mater Sci 1980;15:987–96.
[42] Yamini S, Young RJ. The mechanical properties of epoxy resins. Part 2 Effect of plastic deformation upon crack propagation. J Mater Sci 1980;15:1823–31.
[43] Greenhalgh E. Characterisation of mixed-mode fracture in unidirectional laminates. DRA Technical Report DRA/SMC/CR941003/1.0, Defence Research Agency, Farnborough, 1994.